Ground- and Excited-State Properties of the Mixed-Valence Complex $[(NH_3)_5Ru^{III}NCRu^{II}(CN)_5]^-$

Ivan Kondov,*,† Valérie Vallet,‡ Haobin Wang,§ and Michael Thoss†

Department of Chemistry, Technical University of Munich, 85748 Garching, Germany, Laboratoire PhLAM, UMR CNRS 8523, Université des Sciences et Technologies de Lille, F-59655 Villeneuve d'Ascq, France, and Department of Chemistry and Biochemistry, MSC 3C, New Mexico State University, Las Cruces, New Mexico 88003

Received: February 3, 2008

A computational study of the ground- and excited-state properties of the mixed-valence complex $[(NH_3)_5Ru^{III}NCRu^{II}(CN)_5]^-$ is presented. Employing DFT and TDDFT calculations for the complex in the gas phase and in aqueous solution, we investigate the vibrational and electronic structure of the complex in the electronic ground state as well as the character of the electronically excited states. The relevance of the various excited states for the intervalence metal−metal charge-transfer process in the complex is analyzed based on the change of charge density, spin density, and dipole moment upon photoexcitation as well as by a Mulliken−Hush analysis. Furthermore, those intramolecular modes, which are important for the charge-transfer process, are identified and characterized.

I. Introduction

Photoinduced electron-transfer (ET) reactions in donor−acceptor complexes in solution represent an important class of charge-transfer (CT) processes. In particular, ET reactions in mixed-valence compounds continue to be of interest in this respect.[1–3] These reactions have served as a basic model for the understanding of fundamental mechanisms in ET reactions. A well-studied group of mixed-valence compounds are binuclear complexes of transition metals containing a bridging ligand.[3] In many of these systems, the photoexcitation triggers the exchange of an electron between the two metal centers in different oxidation states. This metal-to-metal charge-transfer (MMCT) reaction manifests itself in a broad asymmetric intervalence absorption band in the visible or near-infrared region.

Probably the best known example of a mixed-valence compound exhibiting intervalence MMCT is the Creutz−Taube ion.[4] The ET process in the Creutz−Taube ion has been studied in detail experimentally[5,6] and theoretically.[7–9] In contrast to the Creutz−Taube complex, other mixed-valence complexes, especially asymmetric complexes (either heteronuclear or homonuclear with different ligands), have not been studied from first principles. The theoretical study of the electronic structure of these complexes is challenging because of the low symmetry of the complexes as well as strong electronic correlation in ground and excited states.

In this paper, we study the binuclear homonuclear complex $[(NH_3)_5Ru^{III}NCRu^{II}(CN)_5]^-$ (RuRu) as an example of an asymmetric mixed-valence compound exhibiting intervalence MMCT. The intervalence MMCT process in RuRu can be expressed by the following reaction scheme

$$[(NH_3)_5Ru^{III}NCRu^{II}(CN)_5]^- \underset{ET}{\overset{h\nu}{\rightleftharpoons}} [(NH_3)_5Ru^{II}NCRu^{III}(CN)_5]^- \quad (1)$$

Upon photoexcitation, an electron is transferred from the ruthenium center in oxidation state II (electron donor) to the other ruthenium center (acceptor) via the cyanide bridge. The processes that follow are vibrational relaxation within the excited state and reverse ET.

The MMCT process in RuRu has been investigated in great detail experimentally in recent years.[10–21] Direct experimental evidence for the ET transition in RuRu was provided by Stark spectroscopy measurements.[18] In this work, a dramatic decrease of the electrostatic dipole moment upon the ET transition was observed, and its implications for the ET mechanism were discussed, calculating the degree of delocalization and the electronic coupling strength. A number of groups have analyzed the MMCT reaction mechanism based on absorption and resonance Raman spectroscopy. Early studies of the electronic absorption spectrum of RuRu in water[12] allowed the estimation of the electronic donor−acceptor coupling in RuRu. Later, resonance Raman spectroscopy studies showed the importance of intramolecular modes of the RuRu complex for the ET reaction.[13,17]

The dynamics of the reverse MMCT reaction in RuRu has been investigated using time-resolved spectroscopy.[15,16,20,21] Femtosecond pump−probe spectra uncovered that the reverse MMCT process takes place on an ultrashort time scale on the order of 100 fs.[15] Employing various rate theories for ET,[22,23] ET parameters were estimated based on resonance Raman and absorption spectra, and the influence of individual intramolecular vibrational modes of the complex on the ET reaction was analyzed.[15] More recently, time- and frequency-resolved femtosecond spectroscopy[20,21] revealed ET times of 80−100 fs in water and provided a global view of the ultrafast ET reaction and other accompanying processes such as stimulated emission and intramolecular and solvent vibrational relaxation. Moreover, the observation of oscillatory features in time-resolved spectroscopic signals indicated the persistence of vibrational coher-

* To whom correspondence should be addressed. Present address: Forschungszentrum Karlsruhe, Hermann-von-Helmholtz-Platz 1, 76344 Eggenstein−Leopoldshafen, Germany. E-mail: ivan.kondov@ch.tum.de.
† Technical University of Munich.
‡ Université des Sciences et Technologies de Lille.
§ New Mexico State University.

10.1021/jp801017m CCC: $40.75
Published on Web 05/21/2008

ence on the ET time scale[21] and raised intriguing questions about the occurrence and observability of vibrational quantum coherence in a condensed-phase environment.

The experimental results have also demonstrated the importance of static and dynamical solvent effects in the RuRu MMCT process.[19–21] The former manifest themselves in large solvent reorganization energies that have strong impact on the free-energy surfaces along the ET reaction coordinate,[19] and the latter result in a dependence of the ET dynamics on the solvents.[20,21]

So far, there have been only very few theoretical studies of the RuRu complex.[24,25] In our previous work,[24,25] we analyzed the dynamics of the ET reaction in RuRu based on a semiempirical ET model, which was parametrized according to experimental data.[13,15] In the present paper, we investigate the electronic and vibronic structure of the RuRu complex based on first-principles electronic structure calculations. Thereby, the focus is on properties that are relevant for the MMCT process in RuRu. We consider both the isolated RuRu complex in the gas phase and the RuRu complex in an aqueous environment. The latter is particularly relevant for a comparison with experimental results.

The remainder of this paper is organized as follows. In section II, we introduce the electronic structure methods used to study the RuRu complex. The results are presented in section III, including the electronic and vibrational structure of the RuRu complex in the electronic ground state, an analysis of the frontier orbitals, simulated infrared spectra, the character of the excited electronic states, as well as a discussion of their relevance for the MMCT process in RuRu based on the change in charge and spin density and a Mulliken−Hush analysis. In addition, we present results for the electronic−vibrational coupling in the electronically excited states of the RuRu complex as well as the corresponding internal reorganization energies of the ET process in RuRu and discuss their manifestation in resonance Raman spectra. Section IV concludes with a summary.

II. Computational Methods

To study the electronic and vibrational structure of RuRu, we have employed density functional theory (DFT). All electronic structure calculations were performed with the program package Turbomole version V5.7.1.[26] Two hybrid density functionals were considered, B3LYP[27] and PBE0,[28] within the unrestricted open-shell model. The choice of these two hybrid functionals was motivated by the fact that they describe the long-range Coulomb interactions better than pure DFT functionals.[29–32] These interactions are important for an accurate description of CT excitations within TDDFT. In particular, these two functionals have been successfully applied to long-range CT excitations in transition-metal complexes and hence recommended for such systems.[32] Because it is a priori not known which functional provides a better description of this specific concrete system, the results with the two functionals will be systematically compared throughout the paper. Several different Gaussian basis sets have been used, including the SVP and the TZVP basis sets from the Turbomole basis set library as well as the LANL2DZ and LANL2DZdp basis sets as retrieved from the EMSL basis set library.[33] Polarization functions are included for all atoms in the SVP and the TZVP basis sets. The LANL2DZ basis set contains no diffuse and polarization functions. The LANL2DZdp basis set is expected to give a better description of ionic states and hydrogen bonds because a diffuse function and a polarization function are included for carbon, nitrogen, and hydrogen. This basis set is characterized by contraction patterns {311/1} for hydrogen, {62111/411/1} for second-row elements, and {31111/411/311} for ruthenium. Relativistic effective core potentials (ECPs) are employed to describe 28 core electrons at each ruthenium center in the complex. With the TZVP and SVP basis sets, the relativistic MWB ECPs[34] from the Turbomole library are used for the two ruthenium atoms. The LANL2DZ and LANL2DZdp basis sets for ruthenium are combined with the Hay−Wadt LANL2DZ ECPs.[35,36]

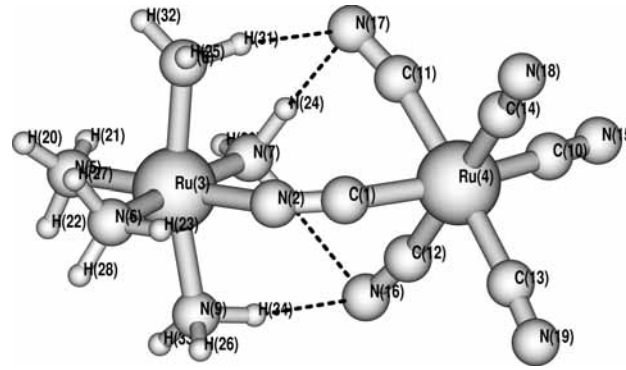

Figure 1. Optimized geometry of the complex in gas phase at the PBE0/TZVP level of theory.

The geometries of the complexes were optimized without symmetry constraints using redundant internal coordinates[37] and considered converged if the norm of the gradient was less than 10^{-4} au. In all optimizations, the criterion for convergence was set to 10^{-8} for the energy and 10^{-7} for the density.

As initial guess for DFT extended Hückel molecular orbitals was used. Alternative use of either the core Hamiltonian eigenfunctions or the molecular orbitals from an unrestricted Hartree−Fock calculation did not alter the converged DFT result.

A normal-mode analysis was performed in the electronic ground state of the complex employing analytic force constant matrices that are available for B3LYP and PBE0 in Turbomole V5.7.1.[38–40] To determine vibrational frequencies including solvent effects, numerical second derivatives were calculated using central differences of analytic first derivatives. To calculate excitation energies and analytic excited-state gradients, the time-dependent DFT (TDDFT) method was used as implemented in Turbomole V5.7.1.[41–45]

Calculations were performed in the gas phase as well as in a polar solvent environment. Motivated by numerous experiments,[10–17,19–21] water was chosen as the solvent. To describe solvent effects, the conductor-like screening model (COSMO)[46] was employed as implemented in Turbomole V5.7.1 for DFT and for TDDFT.[47]

III. Results and Discussion

A. Geometry of the Complex. The geometry of the mixed-valence complex RuRu can be considered as two octahedra on top of each other, sharing the bridging CN ligand (Figure 1). In what follows, we will refer to all NH_3 ligands and nonbridging CN ligands as terminal ligands. The bridging CN ligand and the ligands located at the opposite corner of each octahedron will be distinguished as axial ligands, and the remaining ligands (four per metal center) will be identified as equatorial ligands. The bridging cyanide ligand and the two metallic centers lie in one plane, which will be referred to as the bridge plane. In the Cartesian coordinate system used in all calculations, this is the *xz* plane, where the ruthenium centers are located on the *x* axis.

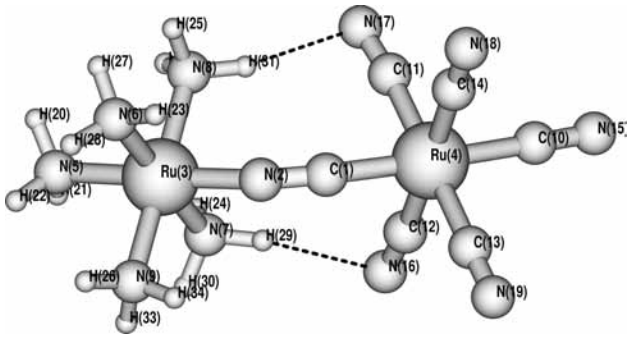

Figure 2. Optimized geometry of the complex in water at the PBE0/TZVP level of theory.

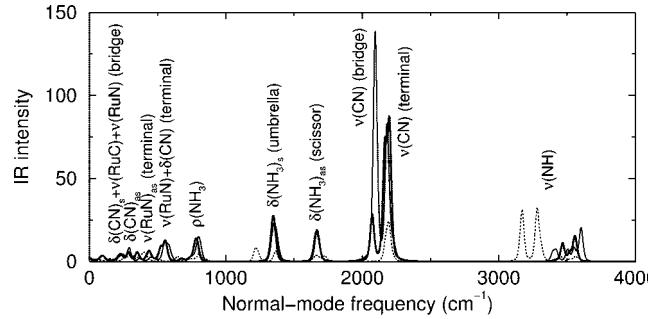

Figure 3. Infrared spectrum of RuRu calculated at the B3LYP/TZVP (thick lines) and PBE0/TZVP levels (thin lines), in water (solid lines) and in the gas phase (dotted lines). A Lorentzian line shape with a broadening of 15 cm $^{-1}$ was used for the representation.

Optimizations with both B3LYP and PBE0 functionals using different basis sets yield very similar structures in the gas phase. The gas-phase calculation using the PBE0 functional together with the TZVP basis set predicts an equilibrium geometry, shown in Figure 1, where the nitrogen atoms of three NH_3 ligands and the axial CN ligand are located in the bridge plane. The octahedral configurations of both ruthenium centers are strongly distorted. Furthermore, the octahedron at Ru(4) is twisted by 49° (as measured by the dihedral angle C(11)−Ru(4)−C(1)−N(2)), and the bridge is strongly bent so that each of the two equatorial CN ligands forms two hydrogen bonds (average length of about 1.97 Å) with equatorial NH_3 ligands. The formation of these four hydrogen bonds makes the bent, distorted structure energetically more favorable than the structure of RuRu with the highest possible symmetry, whereby the octahedra are aligned.

A detailed analysis of the geometry shows that the bending angles of the central Ru−C−N−Ru unit at the bridging carbon and nitrogen atoms are 157 and 144°, respectively, at the PBE0/TZVP level. Very similar results, 158 and 143°, are obtained at the B3LYP/TZVP level. The distance between the two ruthenium centers is 4.7 Å through space and 5.2 Å via the bridging bonds.

The optimized geometry of RuRu in aqueous solution, depicted in Figure 2, differs significantly from that in the gas phase. In particular, the octahedral geometries of both ruthenium centers are regular, and only two hydrogen bonds (between CN at Ru(4) and NH_3 at Ru(3)) are formed. This difference to the gas-phase result can be explained by the rather strong solvent effects (the dielectric solvation energy within the COSMO model is about −13 eV). The formation of intramolecular hydrogen bonds is not favored due to electrostatic screening. The space between the cyanide and ammine ligands is partially filled by the dielectric medium. Thus, the Coulombic interaction between nitrogens and hydrogens is reduced, and hydrogen bonds become less stable.

The detailed analysis of the geometry of the complex in aqueous solution reveals that the bending angles of the central Ru−CN−Ru unit at the bridging carbon and nitrogen atoms are 167 and 152°, respectively. The twisting angles C(11)−Ru(4)−C(1)−N(2) and C(12)−Ru(4)−C(1)−N(2) are 41 and −49°, respectively. In contrast to the structure in the gas phase, where the Ru(3)−octahedron aligns with the bridge plane, in solution, the octahedron at Ru(3) is twisted by −49 and 42° (as measured by the dihedral angles N(8)−Ru(3)−N(2)−C(1) and N(7)−Ru(3)−N(2)−C(1)), respectively. This result demonstrates that taking into account solvent effects can have a significant influence on the spatial structure.

As in the gas phase, optimizations with B3LYP and PBE0 functionals employing different basis sets yield very similar structures. For example, with increasing quality of the basis set (SVP < LANL2DZdp < TZVP), we found only a weak increase of the intermetallic distance, for example, with PBE0 of 4.72, 4.84, and 4.85 Å, respectively. Despite the significant influence of the solvent environment on the spatial structure of the complex discussed above, the intermetallic distance (through space) in water is only about 3% larger compared to that in the gas phase. The somewhat larger distance in water correlates well with the significantly looser hydrogen bonds (average length about 2.29 Å) and their smaller number.

We are not aware of detailed experimental data on the spatial structure of RuRu. The distance between the two ruthenium centers was experimentally determined to 5.0 Å using X-ray diffraction in a crystal environment.[18] This value is slightly larger than the calculated results. It is noted, however, that the intermetallic distance through space depends on the two bond angles at the bridging ligand and thus on the hydrogen bonds. As the number and length of the hydrogen bonds may vary significantly with the environment (gas phase, solution, or crystal lattice), we cannot assess the quality of the optimized structure on the basis of the intermetallic distance alone. A bent structure (similar to the calculated structure in aqueous solution) was found for the related mixed-valence complex, where Ru(4) was replaced by iron and the axial CN ligand by pyridine.[48] In this study, the bent structure detected by X-ray crystallography was attributed to the crystal environment. Our results, however, indicate that this structure is favored both in the gas phase and in a polar solvent environment and thus is not caused (but only influenced) by the environment. As discussed above, the low symmetry of the RuRu complex is due to the formation of multiple intramolecular hydrogen bonds between the cyanide and ammine ligands. This is in contrast to complexes with ammine ligands at both centers (such as the Creutz−Taube complex[7,8]) where the high symmetry is preserved because hydrogen bonds are not formed.

B. Normal-Mode Analysis and Infrared Spectrum. In this section, we consider the vibrational structure of the complex in the electronic ground state based on a normal-mode analysis, as discussed in section II. Figure 3 shows the results of the calculations for the infrared spectrum in the gas phase as well as in water obtained within the harmonic approximation. Table 1 compares selected results to available data from experimental infrared spectra in solid KBr.[11] A complete account of the results from the frequency analysis is given in the Supporting Information.

We first consider the results of the gas-phase calculation (thin dotted lines in Figure 3). The modes contributing significantly to the infrared spectrum can be divided into three groups. The high-frequency region is dominated by symmetric and antisym-

TABLE 1: Calculated and Experimental Vibrational Frequencies (in cm^{-1}) of Selected Vibrational Modes of RuRu[a]

	PBE0/TZVP		B3LYP/TZVP	
mode	gas phase	solvent	solvent	exp.[11]
ν(CN)	2175–2229	2093–2231	2071–2198	2060
$\delta(NH_3)_{as}$	1628–1724	1670	1672	1620
$\delta(NH_3)_s$	1214–1365	1344–1370	1338–1354	1320
$\rho(NH_3)$	777–860	792–815	773–792	810

[a] Multiple modes from the calculation corresponding to one experimental band are given in ranges.

metric ν(NH) stretch modes. This group comprises two types of modes. The first type of modes exhibits a pronounced infrared activity, consists of stretching vibrations of bridging hydrogen atoms, and is seen as two bands at 3171 cm^{-1} (hydrogens at N(8) and N(9)) and 3279 cm^{-1} (hydrogens at N(7)). Each of these two bands includes two individual modes—symmetric and antisymmetric. The second type of high-frequency modes between 3447 and 3590 cm^{-1} contains modes of the remaining hydrogen atoms which are not involved in hydrogen bonds. The latter modes have larger frequencies than the modes of bridging hydrogens and about an order of magnitude lower IR intensity. To our knowledge, there are no available experimental data for the ν(NH) modes of RuRu. Such experimental data could be used to verify the formation of intramolecular hydrogen bonds predicted by our results. The vibrations in the midfrequency range include several ν(CN) and $\delta(NH_3)$ modes. The ν(CN) modes comprise the vibrations of terminal CN ligands at 2175 and 2219 cm^{-1} as well as mixed (bridging + terminal) ν(CN) modes at 2168, 2193, 2208, and 2229 cm^{-1}. Because the mode with frequency 2193 cm^{-1} has a much stronger intensity than the other ν(CN) modes and all ν(CN) modes are very close in frequency, they appear in the (broadened) infrared spectrum as a single band. This is in agreement with experimental results where a single experimental band at the slightly smaller frequency of 2060 cm^{-1} has been assigned to this group of modes.[11] The $\delta(NH_3)$ modes include 10 antisymmetric bending $\delta(NH_3)$ (scissor) modes in the frequency range of 1628−1724 cm^{-1} and symmetric $\delta(NH_3)$ (umbrella) modes at 1214, 1236, and 1365 cm^{-1}. The frequencies of these modes compare rather well to the experimental values[11] of 1620 and 1320 cm^{-1}, respectively. In the frequency range below 1000 cm^{-1}, a number of modes are observed with relatively low intensity. A prominent band is formed by the $\rho(NH_3)$ modes at 777, 807, and 860 cm^{-1}, which is in good agreement with the corresponding experimental band[11] at 810 cm^{-1}.

Due to the different equilibrium structure of the complex, the calculated infrared spectrum in water exhibits noticeable differences compared to that in the gas phase. In the high-frequency region, the ν(NH) modes appear at higher frequencies compared to those in the gas-phase calculation. As was also found in the gas phase, the ν(NH) modes (symmetric at 3395 and 3420 cm^{-1} and antisymmetric at 3551 and 3552 cm^{-1}) of the hydrogen atoms involved in intramolecular hydrogen bonds have higher infrared activity than the other hydrogen atoms. Their frequencies are also weakly shifted with respect to the ν(NH) modes of the hydrogen atoms not involved in hydrogen bonds. This shift is less pronounced than that in the gas phase. In the midfrequency range, the ν(CN) modes appear in three groups: bridging + terminal symmetric at 2231 cm^{-1}, antisymmetric terminal at 2178, 2179, and 2199 cm^{-1}, and bridging at 2093 cm^{-1}. The appearance of a mode which almost exclusively corresponds to the vibration of the bridging CN ligand is also a difference from the result in the gas phase. As discussed above, in the experimental infrared spectrum,[11] the bridging and terminal ν(CN) modes are not detected separately. However, in the postresonance Raman study,[13] the two groups of modes were well distinguished, and the higher-frequency band was attributed to the bridging ν(CN) stretch. This latter assignment, which is in variance with the results of our calculations, was based on the assumption that the bond order in the bridging CN ligand is increased (compared to the other CN ligands), thus increasing the stretching frequency. This assumption cannot be confirmed by our calculations. It is known that the bond order usually correlates well with the stretching frequency as well as with the bond length, for example, the bond order decreases with increasing bond length. Our calculations reveal that the bond length of the bridging CN is larger than the bond lengths of the terminal CN ligands in both the gas phase and water environment. Thus, neither the calculated bond length nor the frequencies of the different ν(CN) modes imply a higher bond order of the bridging CN ligand. This is also confirmed by the character of the frontier orbitals discussed in section III.C. Considering finally the lower-frequency modes, the antisymmetric $\delta(NH_3)$ (scissors) at 1670 cm^{-1} and symmetric $\delta(NH_3)$ (umbrella) at 1344, 1355, and 1370 cm^{-1} as well as the $\rho(NH_3)$ vibrations at 792, 801, and 815 cm^{-1} are in very good agreement with experimental results and with the respective modes calculated in the gas phase.

Table 1 also shows that the frequencies of the vibrational modes discussed above obtained using two different functionals, PBE0 and B3LYP, are in rather good agreement. Moreover, the normal modes do not exhibit qualitative changes with variation of the basis set from LANL2DZ through TZVP (data not shown).

TABLE 2: Frontier Molecular Orbitals of RuRu in the Gas Phase at The PBE0/TZVP Level[a]

β (α) orbital	dominant contribution	energy (eV)	localization
74β occ.	π(CN)	−3.902	terminal
75β occ.	π(CN)	−3.849	terminal
76β occ. (76α occ.)	$d_{xy} + d_{y^2-z^2}$	−3.632 (−3.650)	Ru(3)
77β occ. (77α occ.)	d_{xz}	−3.441 (−3.506)	Ru(3)
78β occ. (78α occ.)	$d_{xy} - d_{y^2-z^2}$	−3.403 (−3.419)	Ru(3)
79β occ. (79α occ.)	$d_{y^2-z^2}$	−2.691 (−3.246)	Ru(4)
80β occ. (81α occ.)	d_{xy}	−2.642 (−2.962)	Ru(4)
81β virt. (80α occ.)	d_{xz}	−0.133 (−2.967)	Ru(4)

[a] For d orbitals, the notation from ref 9 was used.

C. Electronic Structure of the Ground and Excited States. A particularly interesting aspect of mixed-valence compounds, such as the RuRu complex, is the electronic structure in the electronic ground state and the change of the charge distribution upon photoexcitation. In this section, we analyze the electronic structure of the electronic ground state and the character of the electronically excited states and discuss their relevance for the MMCT process observed experimentally.

1. Gas Phase. We first consider the isolated RuRu complex in the gas phase. The electronic ground state of RuRu is a doublet state (D_0).[49] The character of the most relevant molecular orbitals is described in Table 2. The frontier orbitals include the t_{2g} set of d orbitals at both ruthenium centers. The highest occupied molecular orbital (HOMO) is a β orbital of d_π type localized on the Ru(4) center. The single unpaired electron occupies the 80α orbital, which is also localized at Ru(4) but is much lower in energy than the HOMO. To analyze the charge distribution in the electronic ground state, we have performed natural population analysis. Employing the PBE0 functional and

TABLE 3: Excited-State Energies (*E*), Oscillator Strengths (*f*), Occupied Molecular Orbitals (OMO) and Their Contribution (%), and the Character of Excited States of RuRu in the Gas Phase (PBE0/TZVP)[a]

	E (eV)	*f*	OMO	%	character
1	0.31	0.0000	79β	94.6	dark, local
2	0.32	0.0003	80β	93.2	dark, local
3	2.11	0.0015	78β	46.8	dark, MMCT
4	2.12	0.0061	77β	47.4	dark, MMCT
5	2.35	0.0005	74β	70.0	dark, LMCT
6	2.36	0.0153	75β	84.4	bright, LMCT
7	2.38	0.0002	76β	33.5	dark, MMCT
9	2.59	0.0027	78β	22.8	dark, MMCT
10	2.60	0.0105	77β	26.1	bright, MMCT

[a] All excitations occur from the relevant OMO to the LUMO 81β.

TZVP basis set, the natural charge in the ground state, as calculated from the sum of α and β densities, is 0.42 for Ru(3) (the ruthenium center with NH_3 ligands) and 0.03 for Ru(4) (the ruthenium center with CN ligands). The corresponding natural spin populations (from the difference of α and β densities) are 0.01 and 0.81 for Ru(3) and Ru(4), respectively, consistent with the fact that the unpaired electron occupies an orbital localized at Ru(4). Thus, the calculation for the electronic ground state of RuRu in the gas phase predicts that the unpaired electron is localized at the ruthenium center with the CN ligands. This finding is in disagreement with eq 1, which requires that the unpaired electron should be localized on the ruthenium center with the NH_3 ligands (corresponding to an oxidation state of +3).

The character of the doublet excited states of RuRu in the gas phase, based on TDDFT (PBE0/TZVP) calculations, is described in Table 3. All doublet excited states considered involve transitions from the seven highest occupied β orbitals to the lowest unoccupied β orbital (81β, LUMO). Because the LUMO is essentially a d_π orbital (t_{2g} in O(3) symmetry), optically active excitations can arise only from orbitals of the same symmetry, for example, d_{xy} or d_{xz}. The first two electronic excitations (cf. Table 3) correspond to d−d transitions on the same metal center, Ru(4), and carry a very small oscillator strength. Excitations 3 and 4 have MMCT character with dominant direction from Ru(3) to Ru(4). It is noted that this is the opposite of the direction expected from eq 1. Furthermore, the oscillator strength of both excited states is rather small. The oscillator strength of the fourth excited state, D_4, is moderately larger than that of D_3 because D_4 involves the allowed $d_{xz} \rightarrow d_{xz}$ transition (cf. Tables 2 and 3). The natural population analysis of D_4 reveals charges of 0.76 for Ru(3) and −0.20 for Ru(4) and spin populations of 0.41 and 0.46, respectively. The latter corresponds to nearly complete delocalization of the unpaired electron over the two metal centers. The fifth and sixth excited states are ligand-to-metal charge-transfer (LMCT) excitations of the π − d type. While the fifth excited state is dark in absorption, the sixth state has a more than twice larger oscillator strength than the intervalence fourth excitation. These findings are again in disagreement with experimental results which have been obtained in solution.[11,15] In the experimental spectra, there is no indication of large LMCT contributions to the absorption band; all transitions observed are considered as MMCT type with relatively large oscillator strengths.[50] Moreover, the calculated change of dipole moment upon transition from the ground to the fourth excited state is 4.6 D, while the experimental estimate[18] is 13.4 D.

TABLE 4: Frontier Molecular Orbitals of RuRu in Water at the PBE0/TZVP Level[a]

β (α) orbital	principal contribution	energy (eV)	localization
76β occ. (77α occ.)	$d_{y^2-z^2}$ (d_δ)	−7.10(−7.52)	Ru(3)
77β occ. (78α occ.)	− + + + d_{xy} (d_π)	−6.91(−7.23)	Ru(3)
78β occ. (79α occ.)	+ + − − d_{xz} (d_π)	−5.89(−6.01)	Ru(4)
79β occ. (80α occ.)	+ − − + d_{xy} (d_π)	−5.81(−5.88)	Ru(4)
80β occ. (81α occ.)	$d_{y^2-z^2}$ (d_δ)	−5.77(−5.81)	Ru(4)
81β virt. (76α occ.)	+ − − − d_{xz} (d_π)	−3.70(−7.68)	Ru(3)
82β virt. (82α virt.)	d_{x^2} (d_σ)	−0.51(−0.79)	Ru(3)
83β virt. (83α virt.)	d_{yz} (d_σ)	−0.21(−0.58)	Ru(3)
92β virt. (92α virt.)	d_{x^2} (d_σ)	+2.05(+2.03)	Ru(4)
93β virt. (93α virt.)	d_{yz} (d_σ)	+2.07(+2.04)	Ru(4)

[a] For the d_π orbitals, the sign alternation along the bridge direction Ru−N−C−Ru is indicated (cf. Figure 4). For d orbitals, the notation from ref 9 was used.

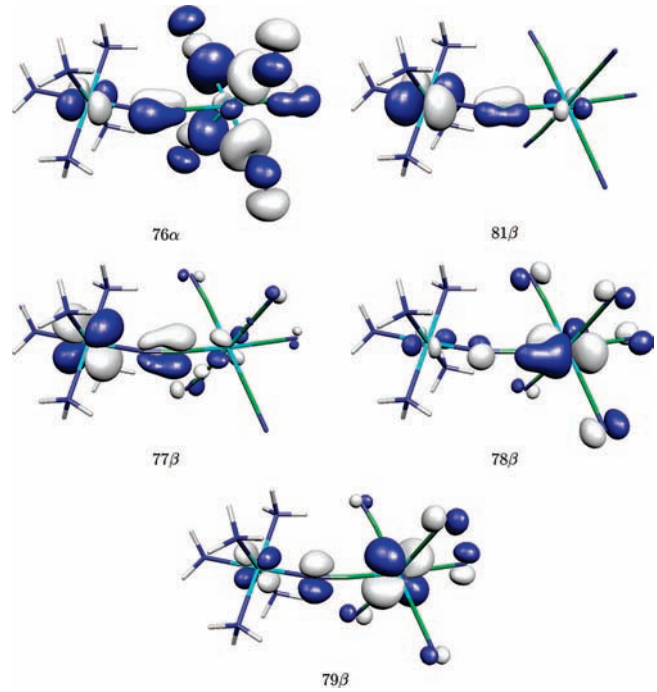

Figure 4. Molecular orbitals calculated at the PBE0/TZVP level in water. Positive and negative signs are depicted by white and blue colors, respectively. The image was created with MOLEKEL.[59]

To summarize, the electronic structures of the ground and excited states of RuRu, as obtained by gas-phase DFT/TDDFT calculations, in particular, the charge and spin distribution in the electronic ground state, the character of the electronically excited states, and the change of electric dipole moment upon excitation, are in disagreement with the experimental results and cannot describe the MMCT process implicit in eq 1. As will be shown below, this disagreement is due to solvent effects, which are not included in the gas-phase calculation.

2. Aqueous Solution. We next consider the electronic structure of the RuRu complex in a water environment as described by the COSMO model. The character of the frontier molecular orbitals, which determine the ground-state[49] as well as excited-state properties, is described in Table 4. The frontier orbitals, which are relevant for the ET process upon photoexcitation, are illustrated in Figure 4. The HOMO (80β) is a d_δ nonbonding orbital localized on Ru(4). The unpaired electron occupies the 76α orbital of d_π character localized on Ru(3). It has much lower energy than the HOMO because it is related to a delocalized five-center π bond (see Figure 4). The LUMO,

TABLE 5: Excited-State Energies (*E*), Oscillator Strengths (f), Occupied Molecular Orbitals (OMO) and Their Contribution (%), and the Character of Excited States of RuRu in Water Obtained at the PBE0/TZVP Level[a]

	E (eV)	*f*	OMO	%	character
1	0.13	0.0000	77β	58.8	dark, local
			79β	36.6	dark, CT
2	0.32	0.0001	76β	97.7	dark, local
3	1.12	0.0010	80β	96.0	dark, CT
4	1.32	0.0698	78β	77.8	bright, CT
			79β	11.1	dark, CT
			77β	6.8	dark, local
5	1.33	0.0183	79β	49.6	dark, CT
			77β	28.2	dark, local
			78β	18.8	bright, CT

[a] All excitations occur from the relevant OMO to the LUMO 81β.

81β, has the same (d_π) character as that in the gas phase but is localized on Ru(3). All results in aqueous solution presented in this work are based on the RuRu geometry optimized in the solvent environment. Nevertheless, it is noted that in the presence of solvent (i.e., the COSMO model is switched on), the orbital occupied by the unpaired electron as well as the LUMO stays localized on Ru(3) also at the geometry optimized in the gas phase. Vice versa, in the absence of solvent, both the LUMO and the unpaired electron are located on Ru(4) in both the gas-phase- and solvent-optimized geometries. Thus, the localization of the unpaired electron is owing predominantly to direct solvent effects but not to geometry effects. However, other properties considered (e.g., intramolecular vibrations) are influenced by both geometric and solvent factors.

Other orbitals that are important for the excitation and ET process include the occupied orbitals 78β and 79β. These two orbitals of d_{xz} and d_{xy} character would be degenerate in the limit of a straight bridge. Due to the bending of the CN bridge in RuRu, the degeneracy of the d_π orbitals is lifted. However, the close orbital energies (energy gap of only 0.08 eV) indicate near degeneracy. The third occupied t_{2g} (d_δ) orbital on Ru(4) has higher energy because its plane is orthogonal to the bridge direction and it cannot take part in the π bonding. Similar behavior of the t_{2g} orbitals has been already found for the Creutz−Taube ion.[9] The last four e_g-type orbitals in Table 4 are vacant. However, they do not contribute to intervalence electronic excitations, as will be shown below.

A natural population analysis on the PBE0/TZVP level (cf. Table 7) reveals charges of 0.85 at Ru(3) and −0.45 at Ru(4) as well as spin populations of 0.87 and 0.1, respectively. This finding is in accordance with the fact that the unpaired electron occupies an orbital localized at Ru(3) and, in contrast to the results of the gas-phase calculations, also in qualitative agreement with eq 1.

In section III.B, we found that the bond order of the bridging C−N bond is decreased in the RuRu complex. This conclusion was based on the bond lengths and vibrational frequencies. To analyze this effect in more detail, we consider now the sign alternation of the occupied orbitals of π-type as shown in Table 4 and in Figure 4. Adjacent sites with the same sign form a π bond. These results indicate that the π bond order of the Ru−C and Ru−N bonds is increased at the expense of the C−N bond order, and the π electrons on CN are partially delocalized, thus confirming the conclusion in section III B. The σ bonds with the ruthenium centers, on the other hand, arise from the nonbonding electrons of CN^- and therefore do not affect the C−N bond order.

TABLE 6: Excited-State Energies (*E*), Oscillator Strengths (*f*), Occupied Molecular Orbitals (OMO) and their contribution (%), and the Character of Excited States of RuRu in Water Obtained at the B3LYP/TZVP Level[a]

	E (eV)	*f*	OMO	%	character
1	0.11	0.0000	79β	58.4	dark, CT
			77β	36.2	dark, local
2	0.40	0.0000	76β	98.3	dark, local
3	0.64	0.0002	80β	72.4	dark, CT
			78β	21.5	bright, CT
4	0.94	0.0003	77β	60.6	dark, local
			79β	33.7	dark, CT
5	1.07	0.1305	78β	76.4	bright, CT
			80β	19.2	dark, CT

[a] All excitations occur from the relevant OMO to the LUMO 81β.

TABLE 7: Natural Charge and Spin Populations on the Metal Centers of RuRu in Water Calculated with Basis Set TZVP[a]

	B3LYP		PBE0		
state	D_0	D_5	D_0	D_4	D_5
charge Ru(3)	0.81	0.75	0.85	0.52	0.52
charge Ru(4)	−0.34	−0.21	−0.45	−0.09	−0.09
spin Ru(3)	0.73	0.53	0.87	0.16	0.15
spin Ru(4)	0.22	0.31	0.10	0.70	0.72

[a] This analysis was performed with Turbomole V5.9.1.

Next, we discuss the character of the excited states of RuRu in aqueous solution. The first five doublet excited states shown in Table 5 include single-electron excitations from different occupied orbitals to the LUMO orbital (81β). A gap of 1.7 eV separates the fifth and the sixth excited states. The first two excitations have very small energies and correspond predominantly to local d−d transitions at the Ru(3) metal center. The third excitation has MMCT character (from Ru(4) to Ru(3)). All three excitations have very low oscillator strengths due to nonmatching symmetries of occupied and virtual (LUMO, 81β) orbitals. The first transitions with larger oscillator strengths are excitations 4 and 5, which both have MMCT character from center Ru(4) to Ru(3). A detailed analysis shows that the lower oscillator strength of the fifth excitation (D_5) is due to the large (about 50%) contribution of the d_{xy} occupied orbital, which does not match the d_{xz}-type LUMO orbital. Nevertheless, the overlap between the d_{xy} and the d_{xz} LUMO is facilitated considerably by the relative twisting of the octahedra of the two metallic centers. As discussed above, the 78β and 79β orbitals that have dominant contributions to the fourth and fifth excited states are almost degenerate. This quasi degeneracy is reflected in the very similar energy of the excited states D_4 and D_5.

All results for the electronic structure of RuRu presented so far have been obtained using the functional PBE0. We note that the use of the B3LYP functional does not alter the character of the frontier orbitals, and therefore, we shall not show numerical data for this case. However, the excited states calculated with the B3LYP functional differ slightly from those obtained with PBE0. The lowest two excited states (Table 6) are identical to those obtained with PBE0. The third excited state, D_3, has considerably (by 0.5 eV) lower energy than that calculated with PBE0 due to a larger contribution of the 78β orbital, but the overall character of this state remains unchanged. The next two states, D_4 and D_5, also have significantly lower energies than those calculated with the PBE0 functional. Due to the dominating contribution of the 77β orbital (and negligible contribution

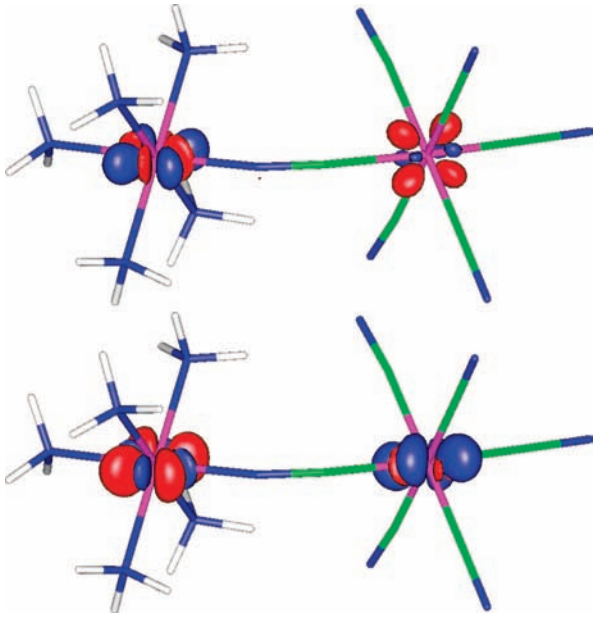

Figure 5. Charge (upper image) and spin (lower image) density difference of the ground and the fifth excited state (D_5) calculated at the PBE0/TZVP level in water. The blue color designates positive and the red color negative change of density, respectively, upon transition to D_5. Images were created with the gOpenMol program.[60]

of the 78β orbital), the state D_4 is local and dark, in contrast to the same state calculated with the PBE0 functional. In contrast, the D_5 state is dominated by the 78β, while the 77β does not contribute to this state. As a result, the state D_5 gains oscillator strength and charge-transfer character. In addition, the degeneracy of the orbitals 78β and 79β discussed above is not transferred to the excited states D_4 and D_5, as is the case using the PBE0 functional. The disagreement between the B3LYP and PBE0 functionals regarding the character and the energies of D_4 and D_5 is presumably due to the quasidegeneracy of the orbitals involved. This problem will be considered in future work. In the following, we shall provide further data with the B3LYP functional only for the D_5 state because only this is relevant for the intervalence transition.

To analyze the MMCT character of the excited states D_4 and D_5 in more detail, we have considered the change in charge and spin density upon photoexcitation and performed natural population analysis. The results in Table 7 obtained at the PBE0/TZVP level are very similar for both excited states. Upon excitation from the ground state, there is a moderate increase of negative charge at Ru(3) by 0.33 and a decrease at Ru(4) by 0.36. This charge transfer is accompanied by a decrease of the spin population at Ru(3) by 0.72 and an increase at Ru(4) by 0.62. The difference of charge (spin) increase and decrease at the two centers indicates a small amount of charge (spin) delocalization. The net transfer of spin (charge) density from the Ru(3) to the Ru(4) center is illustrated in Figure 5 by the difference of spin (charge) density between the ground and excited states. The excitation from the ground state to the excited states D_4 and D_5 thus corresponds to a partial transfer of electronic charge from the metal center Ru(3) to the center Ru(4), and the creation of an electron pair on Ru(3) and is in accordance with the MMCT excitation mechanism in eq 1. The natural population analysis of the data with the B3LYP functional indicates charge and spin population transfer upon electronic excitation that is by a factor of two to six (cf. Table 7) less pronounced than that with the PBE0 functional. In the following, it will be shown that the B3LYP functional behaves in a similar fashion considering the change of electrostatic dipole moment.

TABLE 8: Change of Electric Dipole Moments $\Delta\mu_{12}$ (in Debye) upon Electronic Excitation of RuRu in Water

	B3LYP	PBE0	
basis set	D_5	D_4	D_5
LANL2DZ	−5.4	−11.2	−11.0
SVP	−2.1	−9.7	−9.5
LANL2DZdp	−5.1	−11.2	−11.1
TZVP	−3.9	−11.4	−11.3

TABLE 9: Mulliken−Hush Analysis Based on the PBE0/TZVP Data in Water[a]

state	μ_{11}	μ_{22}	μ_{12}	$\Delta\mu_{12}$	$\lvert\Delta\mu_{ab}\rvert$	H_{ab}	c_b^2	Δq
D_4	74.7	63.3	3.7	−11.4	13.6	0.36	0.082	0.84
D_5	74.7	63.4	1.9	−11.3	11.9	0.21	0.026	0.95

[a] Dipole moments are given in Debye; energies are given in eV.

Though the basic mechanism of the MMCT excitation is reproduced by the calculations, it should be noted that the calculated intervalence excitation energies are significantly lower than the energy of the experimental absorption maximum (1.81 eV).[12,19] Thereby, the results employing the PBE0 (0.5 eV deviation) are closer to experiment than the results obtained with B3LYP (0.8 eV deviation). This underestimation of the excited-state energies is presumably due to the deficiency of TDDFT in treating long-range CT excitations.[29,32] In particular, this artifact has been found in low-symmetry transition-metal complexes with electron-rich ligands (such as CN^- in this work).[32] Another factor for the underestimated excitation energies can be the neglect of fast relaxation of solvent polarization (nonequilibrium effects) in the COSMO model used.[46,47] The error due to neglect of nonequilibrium effects was found to be up to 10% for polar solvents[47] and is expected to be smaller than that due to the TDDFT deficiency outlined above. More recently, it was also shown[51] that relative solvatochromic shifts are weakly influenced by this approximation, and the use of a more accurate method does not change the shifts qualitatively.

It is also noted that although there is significant change in spin density at the two ruthenium centers upon photoexcitation, the amount of charge transfer is relatively small. However, the experimental estimate for the charge transfer is based on the change in dipole moment rather than the amount of charge transferred between the ruthenium centers. The direct correlation of the change of the dipole moment with the change of atomic charge on the ruthenium centers neglects possible relocation of charge to other atoms. As will be discussed in more detail at the end of this section, there are indications for delocalization of charge for the relevant electronic excitations.

The ET between the ruthenium centers upon excitation manifests itself also in a change of the dipole moment. As shown in Table 8, all functionals and basis sets used predict a significant decrease of the dipole moment upon photoexcitation, that is, the excited states are less polar than the ground state. Thereby, as to be expected from purely electrostatic considerations, the direction of the dipole moment is almost unchanged (the change of the projection along the x axis is more than 99.9% of the change of the total vector length with both functionals and all basis sets). The results employing the PBE0 functional, which give a decrease in dipole moment from −10 up to −11 D (depending on the basis set used), are in rather good agreement

TABLE 10: Frequencies and Reorganization Energies (both in cm^{-1}) of Selected Raman-Active Modes Calculated at the PBE0/TZVP Level in Water

	theoretical					experimental[13,15]				
	D_0	D_4		D_5			ref 13		ref 15	
mode	ω	Δ	λ	Δ	λ	ω	$\lvert\Delta\rvert$	λ	$\lvert\Delta\rvert$	λ
$\nu(CN)_{bridging}$	2093	0.73	564	0.76	598	2118	0.93	920	0.68	484
$\nu(CN)_{terminal}$	2231	0.30	98	0.30	100	2077	0.49	250	0.36	135
$\nu(Ru-CN)_{terminal} + \delta(RuCN)$[a]	548	−0.72	141	−0.79	169	565	1.43	580	1.05	313
$\nu(Ru-CN)_{bridge} + \delta(RuCN)$[b]	602	0.67	137	0.66	129	539	1.56	660	1.16	363
$\nu(Ru-NH_3)_{axial}$[c]	468	0.33	26	0.25	15	492	1.19	350	0.88	189
$\nu(Ru-NH_3)_{axial}$	445	−0.27	17	−0.32	23	470	0.90	190	0.67	107
$\nu(Ru-NC)$						355	0.98	170	0.73	95
$\delta(RuNC) + \nu(Ru-NC) + \nu(Ru-CN)$	291	2.29	755	2.22	718					
$\delta(H_3N-Ru-NH_3)$[d]	221	−0.53	32	−0.69	53	270	2.52	860	1.89	483
$\delta(H_2N-Ru-NC) + \delta(NC-Ru-CN) + \delta(RuNC)$	142	−2.36	397	−2.54	459					
total			2167		2264			3980		2169

[a] In this work, $\nu(Ru-CN)_{axial} + \delta(RuCN)_{equatorial} + \nu(Ru-NC)$, [b] In this work, $\nu(Ru-CN)_{bridge} + \delta(RuCN)_{terminal} + \nu(Ru-NC)$. [c] In this work, $\nu(Ru-NH_3)_{all}$. [d] In this work, also 240 and 275 cm^{-1}.

with the experimental estimate of 13.4 D obtained from Stark spectroscopy.[18] This value corresponds to an adiabatic CT distance of 2.2 Å that compares very well with the experimental value of 2.8 Å. Note that this effective distance is about 55% shorter than the geometric distance (4.8 Å). A significant mismatch between the geometric and CT distance has been found by Vance et al.[18] The change of the dipole moment upon photoexcitation obtained with the B3LYP functional, on the other hand, is significantly smaller than the experimental result. This is consistent with the larger deviation of the excitation energies and with the remarkably smaller charge and spin populations transferred between the ruthenium centers found with the B3LYP functional. In the following, we will therefore only consider results based on the PBE0 functional.

Within an idealized model with point charges at the atoms, where only the charges on the two ruthenium centers are allowed to vary, a dipole moment decrease of 11 D corresponds to the transfer of about half of an electron charge from Ru(3) to the Ru(4) (using the geometric through-space distance of 4.8 Å between the ruthenium centers). To use the geometric distance for calculating the transferred charge, one assumes that locations of both donor and acceptor centers coincide with the ruthenium nuclei. Another possible reason for the small CT distance may be partial delocalization of charge upon optical excitation. Therefore, instead of the geometric distance, one should consider both the adiabatic and the diabatic CT distances to estimate the effective charge transferred (the ratio of the two CT distances is equal to the charge transferred, Δq).

By definition, the adiabatic CT distance R_{12} corresponds to the change of the adiabatic dipole moment $\Delta\mu_{12} = eR_{12}$, while the diabatic CT distance R_{ab} is related to the change of the diabatic dipole moment $\Delta\mu_{ab} = eR_{ab}$, where e is the unit charge. We have applied the generalized Mulliken−Hush method[52] to calculate the change of the diabatic dipole moment $\Delta\mu_{ab}$ and the electronic coupling H_{ab} by diagonalizing the dipole moment matrix for each pair of adiabatic states (ground and excited). Thereby, the change of the diabatic dipole moment $\Delta\mu_{ab}$ is given by the difference of the eigenvalues. The dipole moment matrix is readily constructed from the calculated (adiabatic) values for the dipole moments of the ground state μ_{11}, excited state μ_{22}, and the transition dipole moment μ_{12}. Besides the electronic coupling element $H_{ab} = \mu_{12}\Delta E_{12}/\Delta\mu_{ab}$, where ΔE_{12} denotes the excitation energy, we consider the Hush mixing coefficient $c_b^2 = 0.5(1 - \Delta\mu_{12}/\Delta\mu_{ab})$.[1,18] This coefficient is a measure for the delocalization of the electronic wave function. A mixing coefficient of $c_b^2 = 0.5$ corresponds to complete delocalization, while $c_b = 0$ corresponds to complete localization. The results of the analysis are summarized in Table 9.

For both states D_4 and D_5, calculated using of PBE0 functional, the change of the diabatic dipole moment does not significantly differ from the corresponding adiabatic difference (cf. Table 9). This is in agreement with previous work,[18] where it was also found that the CT distances are only marginally changed after diabatization. The electronic coupling for D_4 of $\approx$2900 cm^{-1} compares better to the experimental estimate (3000 cm^{-1}) than the coupling of the D_5 state ($\approx$1700 cm^{-1}). The mixing coefficients for both states are in very good agreement with those from ref 18 (0.039) and with the assignment of RuRu to class II in the Robin−Day classification for intervalence compounds,[1] that is, weak delocalization. The corresponding transferred charges are $\Delta q = 0.84$ and 0.95 ($\Delta q = 1 - 2c_b^2$) for transitions to D_4 and D_5, respectively.

It should be emphasized, however, that the classification based on the Mulliken−Hush method as employed here is an approximate concept. First, we have only included two electronic states in the analysis. The electronic structure results, however, indicate that other closely lying electronic states may influence the result. Second, the definition of diabatic states by diagonalizing the dipole moment matrix, as employed in the Mulliken−Hush method, may not be appropriate for optical CT transitions considered here because the diabatic transition dipole moment vanishes.

D. Electronic−Vibrational Coupling and Resonance Raman Spectra. In section III.C, we discussed the electronically excited states of RuRu on the basis of excitation energies at a fixed nuclear geometry. As is well-known, to study optical spectra (e.g., absorption or resonance Raman spectra) or dynamics in electronically excited states, the coupling to the nuclear degrees of freedom has to be taken into account. To account for this effect, the potential energy, $V_n(Q)$, of the nth electronic state is expanded about the equilibrium geometry of the electronic ground state

$$V_n(Q) = E_n + \sum_l \kappa_l^{(n)} Q_l + \sum_{lk} \gamma_{lk}^{(n)} Q_l Q_k \qquad (2)$$

Here, E_n denotes the energy of the nth excited state at the equilibrium geometry of the electronic ground state, and Q_l is the lth normal mode in mass-scaled coordinates.

In the simplest approximation, only the linear term of the expansion is taken into account; the frequencies are ap-

proximated by their ground-state values, and Duschinsky rotation[53] of the normal modes is neglected. In this way, we obtain

$$V_n(Q) = E_n + \sum_l \kappa_l^{(n)} Q_l + \frac{1}{2}\sum_l \omega_l^2 Q_l^2 \quad (3)$$

where ω_l denotes the frequency of the normal mode Q_l in the electronic ground state. This approximation has been used successfully to describe Franck−Condon and resonance Raman spectra.[54] It is also used in the linear vibronic coupling model of conical intersections[55] and in the Marcus theory of ET.[56]

The electronic−vibrational coupling parameter $\kappa_l^{(n)}$ is related to the reorganization energy of the lth mode, $\lambda_l^{(n)}$, via

$$\lambda_l^{(n)} = \frac{1}{2}\left(\frac{\kappa_l^{(n)}}{\omega_l}\right)^2 = \frac{1}{2}(\omega_l \Delta_l^{(n)})^2 \quad (4)$$

where $\Delta_l^{(n)}$ denotes the displacement of the minimum of the nth electronic state relative to the ground-state minimum along the normal mode Q_l. The total internal reorganization (stabilization) energy of the nth electronic state, $\lambda^{(n)}$, is given as the sum over all normal modes, $\lambda^{(n)} = \sum_l \lambda_l^{(n)}$. This parameter describes the energy related to the relaxation of the nuclear degrees of freedom from the equilibrium geometry of the ground electronic state to the one of the nth electronic state. Here, we will analyze the importance of electronic−vibrational coupling in the excited states D_4 and D_5 based on the electronic−vibrational coupling parameters $\kappa_l^{(n)}$ and the corresponding reorganization energies $\lambda_l^{(n)}$ in these two states.

As is implied in eq 2, the electronic−vibrational coupling strengths $\kappa_l^{(n)}$ are given as the gradients of the potential energy of the nth electronic state with respect to the normal mode Q_l at the equilibrium geometry of the electronic ground state

$$\kappa_l^{(n)} = \left(\frac{\partial E_n}{\partial Q_l}\right)_0 \quad (5)$$

In our practical implementation, $\kappa_l^{(n)}$ is calculated efficiently from the analytic Cartesian gradients of the energy

$$\kappa_l^{(n)} = \sum_{i=1}^{3N} \left(\frac{\partial E_n}{\partial x_i}\right)_0 m_i^{-1/2} \tilde{U}_{il} \quad (6)$$

Here, N is the number of atoms in the complex, x_i denote the Cartesian nuclear coordinates, m_i are the atomic masses pertaining to x_i, and $\tilde{U}_{il}$ are the components of the lth eigenvector of the mass-scaled Hessian matrix

$$\tilde{f}_{ij} = \left(\frac{\partial^2 E_0}{\partial x_i \partial x_j}\right)_0 m_i^{-1/2} m_j^{-1/2} \quad (7)$$

The latter is taken at the reference geometry, that is, the geometry of the optimized ground state.

Using this method, the electronic−vibrational coupling constants and the reorganization energies pertaining to all individual normal modes of RuRu were calculated for the fourth (D_4) and the fifth (D_5) excited states, which contribute to the intervalence MMCT band. Because of the better agreement with experimental results and with the basic MMCT mechanism, we will restrict the discussion to results obtained for RuRu in aqueous solution. The total internal reorganization energies calculated with different basis sets are summarized in Table 11. The data with the two larger basis sets, LANL2DZdp and TZVP, agree within 1%. Because the relaxation energy in the D_5 state is about 400 cm^{-1} larger than that in D_4, the minimum of D_5 is located, within the harmonic approximation, lower than the minimum of the D_4 state. Thus, the D_4 and D_5 energy surfaces are expected to cross in a certain region. The results for the most strongly coupled modes are given in Table 10. The two selected excited states are characterized by very similar values for the vibronic coupling strengths. The modes with the largest electronic−vibrational coupling strengths include the high-frequency CN stretch vibration of the bridge, two ν(Ru−CN) + δ(RuCN) modes in the midfrequency range, as well as two low-frequency vibrations of the bridging moiety, the δ(RuNC) +ν(Ru−NC)+ν(Ru−CN)andtheδ(H_2N−Ru−NC)+δ(NC−Ru−CN) + δ(RuNC). The most relevant of these modes are illustrated in Figure 6. The total internal reorganization energy of RuRu (including all 96 modes) is 4061 cm^{-1} in the D_5 electronic state and 3656 cm^{-1} in D_4. The eight most strongly coupled modes thus account for approximately 60% of the total internal reorganization energy.

TABLE 11: Total Internal Reorganization Energies (in cm^{-1}) of Selected Excited States in Water Obtained within the Harmonic Approximation (equation 3)[a]

level	D_4	D_5
PBE0/SVP	4208	4019 (2570)
PBE0/LANL2DZdp	3640	4102
PBE0/TZVP	3656	4061 (2170)

[a] The relaxation energies based on the optimization of the excited states are given in brackets for cases in which data are available.

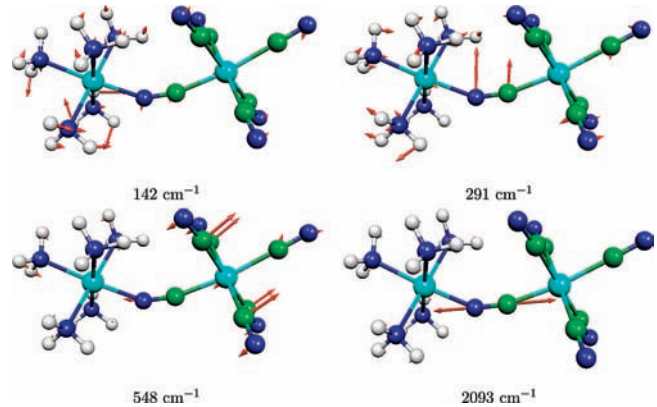

Figure 6. Graphical representation of selected normal modes in water with strong electronic−vibrational coupling (cf. Table 10).

The calculated results are compared in Table 10 to two different experimental results.[13,15] Both experimental results are based on the same postresonance Raman spectrum.[13] The frequencies observed in the postresonance Raman spectrum as well as the corresponding assignments are in rather good agreement with the results of our calculations. To determine the corresponding internal reorganization energies from the experimental results, in addition to the postresonance Raman spectrum, the width of the absorption spectrum was taken into account. Thereby, slightly different approaches were followed in refs 13 and 15. In ref 13, the width of the absorption spectrum was attributed to eight intramolecular modes, thereby neglecting the contribution of the polar solvent to the broadening. This results in a relatively large internal reorganization energy of 3980 cm^{-1}. Although this value is in rather good agreement with the total internal reorganization energy obtained in the calculation, it significantly overestimates the electronic−vibrational coupling in the eight modes observed. On the basis of the same resonance Raman spectrum, in ref 15, the absorption spectrum of RuRu in water was simulated with the solvent-induced broadening as an additional adjustable parameter. The latter

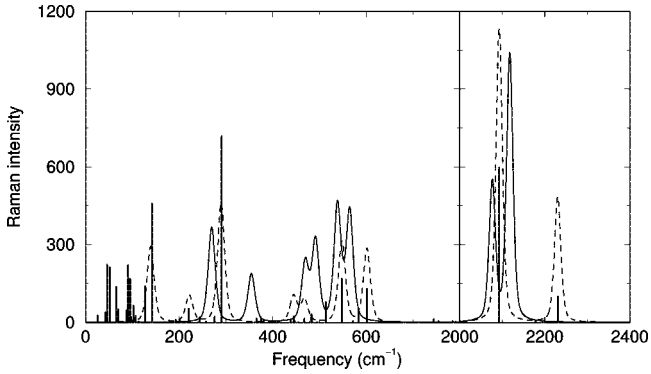

Figure 7. Reorganization energies (shown as sticks) in the fifth doublet excited state (D_5) calculated at the PBE0/TZVP level in water. Dashed lines show Raman spectra calculated from the normal modes shown in Table 10 using the relation $I_k/I_l = |\kappa_k/\kappa_l|$, and solid lines show the Raman spectra reconstructed from ref 15, both with Lorentzian broadening of 8 cm^{-1}.

model results in significantly smaller reorganization energies for the eight most strongly coupled vibrational modes and compares rather well to our calculated results, as seen in Table 10.

A direct comparison of experimental and theoretical results requires the simulation of resonance Raman and absorption spectra. This involves dynamical simulations including the intramolecular nuclear degrees of freedom and the influence of the solvent. Such a dynamical simulation is beyond the scope of the present paper. Here, a first estimate of the resonance Raman spectrum, which still allows us to compare to experimental data, can be obtained based on the short-time approximation[57,58] for the relative intensities using the relation $I_k/I_l = |\kappa_k/\kappa_l|$. Figure 7 shows a comparison of calculated intensities of nine modes with experimental results, which have been reconstructed using the frequencies and reorganization energies from ref 15.

Despite the good agreement of the total internal reorganization energies, a detailed analysis of the mode-specific values and the comparison of the approximate resonance Raman spectra in Figure 7 reveal a number of deviations between experimental and theoretical results. In contrast to the experimental results, the calculated frequency of the bridge ν(CN) mode is lower than the frequencies of the terminal ν(CN) modes. As discussed in section III.B, this is due to the decreased bond order of the bridging CN bond. In addition, the ν(Ru−NC) mode cannot be identified as a single normal mode in our results. Instead, it is mixed with the ν(Ru−CN), δ(RuCN), and δ(Ru−NC) modes (see Table 10). We found three $\delta(H_3N-Ru-NH_3)$ modes with total reorganization energy one order of magnitude smaller than that for the single mode obtained in the experimental results. Furthermore, the calculations predict a strongly coupled low-frequency $\delta(H_2N-Ru-NC) + \delta(NC-Ru-CN) + \delta$(RuNC) mode ($\omega$ = 142 cm^{-1}), which was not observed in the postresonance Raman spectrum of ref 15. More recently, however, a mode with a similar frequency of 160 cm^{-1} was observed in resonance Raman spectra of RuRu in water.[17] This mode is presumably also responsible for the oscillatory structure observed in pump−probe signals of RuRu in different solvents.[20,21]

Finally, it is noted that the difference between the Franck−Condon energy and the excited-state minimum energy is significantly smaller than the total internal reorganization energy determined within the harmonic approximation (see Table 11). This finding is an indication that effects due to anharmonicity, mode mixing, and conical intersection may be of importance in this system. These effects will be the subject of a future study.

IV. Conclusions

In this paper, we have presented a computational study of the binuclear ruthenium complex $[(NH_3)_5Ru^{III}NCRu^{II}(CN)_5]^-$. Employing DFT and TDDFT methods, the spatial and electronic structure of the electronic ground state, the character of the electronic excitations, the vibrational structure of the complex, as well as the electronic−vibrational coupling have been analyzed. The calculations have been performed for the complex in the gas phase as well as in aqueous solution.

The results of the study can be summarized as follows. The complex exhibits a bent geometrical structure in both the gas phase and aqueous solution. Thereby, the alignment of the ligands of the two metal centers as well as the number of hydrogen bonds formed within the complex depends on the environment. The infrared spectra obtained based on a vibrational analysis are overall in good agreement with experimental results. The analysis of the electronic structure of the ground and excited states shows a significant influence of the environment. While the calculation for the RuRu complex in the gas phase predicts localization of the unpaired electron on the ruthenium center with the cyanide ligands, the results obtained in water predict localization on the center with ammine ligands. Furthermore, in the gas phase, all optical electronic excitations with MMCT character are accompanied by a change of charge and spin density that is in contradiction with the basic MMCT schema of eq 1. In contrast, the calculations in the aqueous environment exhibit charge-transfer excitations and changes in charge and spin density that are in qualitative agreement with the MMCT schema (eq 1). Especially, the change of dipole moment upon excitation of 11 D in aqueous solution is in good agreement with experimental results. Thus, the inclusion of the solvent environment in the electronic structure model is of essential importance for the study of the RuRu complex. A Mulliken−Hush analysis revealed that the complex belongs to class II of the Robin−Day classification of intervalence compounds, that is, weak delocalization.

Furthermore, we have investigated the electronic−vibrational coupling in those electronic states of the complex that are relevant for the intervalence MMCT process. In particular, we have calculated the reorganization energies of all intramolecular modes in the intervalence excited states and analyzed which modes are important for the ET process and resonance Raman spectra. The total reorganization energy of the spectroscopically relevant modes was found to be in very good agreement with empirical models based on experimental results.[13,15] However, the significant mismatch between the total internal reorganization energy calculated using the harmonic approximation and the relaxation energy to the excited-state minimum indicates that anharmonic effects might be important for the ET process in RuRu.

In the present work, we have concentrated on the static aspects of the MMCT process in the RuRu complex. The investigation of the dynamics of the ET process requires a construction of diabatic potential energy surfaces as well as multidimensional quantum dynamical simulations. This will be the subject of future work.

Acknowledgment. I.K. and M.T. would like to thank Wolfgang Domcke for helpful discussions. Generous allocation of computing time by the Leibniz Computing Center (LRZ) and the Computing Center of the Max-Planck Gesellschaft (Garching) is gratefully acknowledged. This work has been supported by the Deutsche Forschungsgemeinschaft (DFG). H.W. also acknowledges the NSF CAREER award CHE-0348956 for partial support of this research.

Supporting Information Available: Cartesian atomic coordinates, normal-mode frequencies, and infrared intensities of the optimized RuRu in water environment. This material is available free of charge via the Internet at http://pubs.acs.org.

References and Notes

(1) Robin, M. B.; Day, P. *Adv. Inorg. Chem.* **1967**, *10*, 247.
(2) Allen, G. C.; Hush, N. S. *Prog. Inorg. Chem.* **1967**, *8*, 357.
(3) Creutz, C. *Prog. Inorg. Chem.* **1983**, *30*, 1.
(4) Creutz, C.; Taube, H. *J. Am. Chem. Soc.* **1969**, *91*, 3988.
(5) Rocha, R. C.; Brown, M. G.; Londergan, C. H.; Salsman, J. C.; Kubiak, C. P.; Shreve, A. P. *J. Phys. Chem. A* **2005**, *109*, 9006.
(6) Dinolfo, P. H.; Williams, R. D.; Hupp, J. T. *Chem. Phys.* **2005**, *319*, 28.
(7) Bencini, A.; Ciofini, I.; Daul, C. A.; Ferretti, A. *J. Am. Chem. Soc.* **1999**, *121*, 11418.
(8) Chen, Z.; Bian, J.; Zhang, L.; Li, S. *J. Chem. Phys.* **1999**, *111*, 10926.
(9) Bolvin, H. *J. Phys. Chem. A* **2003**, *107*, 5071.
(10) Meyer, T. J. *Acc. Chem. Res.* **1978**, *11*, 94.
(11) Siddiqui, S.; Henderson, W. W.; Shepherd, R. E. *Inorg. Chem.* **1987**, *26*, 3101.
(12) Burewicz, A.; Haim, A. *Inorg. Chem.* **1988**, *27*, 1611.
(13) Doorn, S. K.; Hupp, J. T. *J. Am. Chem. Soc.* **1989**, *111*, 1142.
(14) Dong, Y.; Hupp, J. T. *Inorg. Chem.* **1992**, *31*, 3170.
(15) Tominaga, K.; Kliner, D. A. V.; Johnson, A. E.; Levinger, N. E.; Barbara, P. F. *J. Chem. Phys.* **1993**, *98*, 1228.
(16) Doorn, S. K.; Dyer, R. B.; Stoutland, P. O.; Woodruff, W. H. *J. Am. Chem. Soc.* **1993**, *115*, 6398.
(17) Bignozzi, C. A.; Argazzi, R.; Strouse, G. F.; Schoonover, J. R. *Inorg. Chim. Acta* **1998**, *275*−*276*, 380.
(18) Vance, F. W.; Karki, L.; Reigle, J. K.; Hupp, J. T.; Ratner, M. A. *J. Phys. Chem. A* **1998**, *102*, 8320.
(19) Sanchez-Burgos, F.; Galan, M.; Dominguez, M.; Perez-Tejeda, P. *New J. Chem.* **1998**, *22*, 907.
(20) Kambhampati, P.; Son, D. H.; Kee, T. W.; Barbara, P. F. *J. Phys. Chem. A* **2000**, *104*, 10637.
(21) Son, D. H.; Kambhampati, P.; Kee, T. W.; Barbara, P. F. *J. Phys. Chem. A* **2002**, *106*, 4591.
(22) Jortner, J.; Bixon, M. *J. Chem. Phys.* **1988**, *88*, 167.
(23) Sumi, H.; Marcus, R. A. *J. Chem. Phys.* **1986**, *84*, 4894.
(24) Wang, H.; Thoss, M. *J. Phys. Chem. A* **2003**, *107*, 2126.
(25) Thoss, M.; Kondov, I.; Wang, H. In *Quantum Dynamics of Complex Molecular Systems*; Micha, D. A. , Burghardt, I. , Eds.; Springer Series in Chemical Physics Vol. 83; Springer: Berlin, 2007; p 195.
(26) Ahlrichs, R.; Bär, M.; Häser, M.; Horn, H.; Kölmel, C. *Chem. Phys. Lett.* **1989**, *162*, 165.
(27) Becke, A. D. *J. Chem. Phys.* **1993**, *98*, 5648.
(28) Perdew, J. P.; Ernzerhof, M.; Burke, K. *J. Chem. Phys.* **1996**, *105*, 9982.
(29) Dreuw, A.; Weisman, J. L.; Head-Gordon, M. *J. Chem. Phys.* **2003**, *119*, 2943.
(30) Dreuw, A.; Head-Gordon, M. *Chem. Rev.* **2005**, *105*, 4009.
(31) Cramariuc, O.; Hukka, T. I.; Rantala, T. T.; Lemmetyinen, H. *J. Phys. Chem. A* **2006**, *110*, 12470.
(32) Vlček, A., Jr.; Záliš, S. *Coord. Chem. Rev* **2007**, *251*, 258.
(33) EMSL Basis Set Library, Environmental and Molecular Sciences Laboratory, Pacific Northwest Laboratory, 2006; URL: http://www.emsl.pnl.gov/.
(34) Andrae, D.; Haeussermann, U.; Dolg, M.; Stoll, H.; Preuss, H. *Theor. Chim. Acta* **1990**, *77*, 123.
(35) Dunning, T. H., Jr.; Hay, P. J. *Methods of Electronic Structure Theory*, 3rd ed.; Plenum Press: New York, 1977; Vol. 2.
(36) Ortiz, J. V.; Hay, P. J.; Martin, R. L. *J. Am. Chem. Soc.* **1992**, *114*, 2736.
(37) von Arnim, M.; Ahlrichs, R. *J. Chem. Phys.* **1999**, *111*, 9183.
(38) Horn, H.; Weiss, H.; Häser, M.; Ehrig, M.; Ahlrichs, R. *J. Comput. Chem.* **1991**, *12*, 1058.
(39) Deglmann, P.; Furche, F.; Ahlrichs, R. *Chem. Phys. Lett.* **2002**, *362*, 511.
(40) Deglmann, P.; Furche, F. *J. Chem. Phys.* **2002**, *117*, 9535.
(41) Weiss, H.; Ahlrichs, R.; Häser, M. *J. Chem. Phys.* **1993**, *99*, 1262.
(42) Bauernschmitt, R.; Ahlrichs, R. *Chem. Phys. Lett.* **1996**, *256*, 454.
(43) Bauernschmitt, R.; Häser, M.; Treutler, O.; Ahlrichs, R. *Chem. Phys. Lett.* **1997**, *264*, 573.
(44) Grimme, S.; Furche, F.; Ahlrichs, R. *Chem. Phys. Lett.* **2002**, *361*, 321.
(45) Furche, F.; Ahlrichs, R. *J. Chem. Phys.* **2002**, *117*, 7433.
(46) Eckert, F.; Klamt, A. *AIChE J.* **2002**, *48*, 369.
(47) Cossi, M.; Barone, V. *J. Chem. Phys.* **2001**, *115*, 4708.
(48) Vance, F. W.; Slone, R. V.; Stern, C. L.; Hupp, J. T. *Chem. Phys.* **2000**, *253*, 313.
(49) The expectation value of the total spin squared $\langle S^2 \rangle$ is at most 1.4% larger than 3/4 for each basis set and functional used. Thus, the ground state is practically a pure doublet.
(50) Crutchley, R. J. *Adv. Inorg. Chem.* **1994**, *41*, 273.
(51) Cammi, R.; Corni, S.; Mennucci, B.; Tomasi, J. *J. Chem. Phys.* **2005**, *122*, 104513.
(52) Cave, R. J.; Newton, M. D. *Chem. Phys. Lett.* **1996**, *249*, 15.
(53) Duschinsky, F. *Acta Physicochim. URSS* **1937**, *7*, 551.
(54) Myers, A. B. *Chem. Rev.* **1996**, *96*, 911.
(55) Domcke, W., Yarkony, D. R., Köppel, H., Eds.; Advanced Series in Physical Chemistry, Vol. 15; World Scientific: Singapore, 2004.
(56) Marcus, R. A.; Sutin, N. *Biochim. Biophys. Acta* **1985**, *811*, 265.
(57) Heller, E.; Sundberg, R.; Tannor, D. *J. Phys. Chem.* **1982**, *86*, 1822.
(58) Myers, A. *Chem. Rev.* **1996**, *96*, 911.
(59) Flükiger, P.; Lüthi, H. P.; Portmann, S.; Weber, J. *Molekel 4.3.*; 2000.
(60) Laaksonen, L. *gOpenMol 2.32* ; 1999.

JP801017M